Journal of Taibah University for Science xxx (2016) xxx–xxx
www.elsevier.com/locate/jtusci

Comparison of different geometric configurations and materials for neutron radiography purposes based on a ^{241}Am/Be neutron source

J.G. Fantidis

Department of Electrical Engineering, Eastern Macedonia and Thrace Institute of Technology, Kavala, Greece

Received 4 April 2016; received in revised form 15 August 2016; accepted 2 October 2016

Abstract

The present work examines two different geometric configurations and three different lining materials that are suitable for thermal neutron radiography purposes based on a ^{241}Am/Be neutron source. The same source was also used for fast neutron radiography. Appropriate collimators were simulated for each of the radiography modes, comparing the effectiveness of Cadmium, Gadolinium, and Boral as lining materials for thermal neutron radiography and evaluating the efficiency of Iron and Tungsten as interior wall materials of the collimator in the case of fast neutron radiography. The presented facilities have been simulated for a wide range of parameter values to characterize neutron radiography using the MCNP4B Monte Carlo code.

Keywords: Monte Carlo simulations; Thermal neutron radiography; Fast neutron radiography; ^{241}Am/Be

1. Introduction

Neutron radiography (NR) is a powerful non- destructive method that works in the same way as X- or gamma ray imaging techniques, but exploits a neutron beam instead. The method has been established as a non-destructive technique and as a research tool for over 70 years and is usually used in security applications, engineering studies and industry to determine structural defects as well as in geology, medicine and biological research [1–7].

Because of the availability of high-intensity thermal neutron beams from nuclear research reactors and based on the fact that thermal neutrons interact with various materials with very specific cross-sections that are largely independent of the atomic number (Z) of the material, thermal NR has been thoroughly developed and is commercially available. However, for objects with more than a few centimeters of thickness, the use of neutrons with higher energies is necessary. Fast neutrons that have an energy higher than 1 MeV have considerably higher penetrating capabilities, but have smaller differences in cross section from element to element, and are able to offer the prospect of expanding the range of NR applications [8].

Both in thermal and fast NR, high flux neutron sources and well-collimated neutron beams are the main essential

E-mail address: fantidis@yahoo.gr
Peer review under responsibility of Taibah University.

Production and hosting by Elsevier

http://dx.doi.org/10.1016/j.jtusci.2016.10.002

components of a high performance neutron radiography facility. The primary goals of this work are to find the optimum design and materials for neutron collimators based on neutrons from a ^{241}Am/Be source. All of the proposed designs have been simulated using the MCNP4B Monte Carlo code [9].

2. Materials and methods

2.1. Neutron source

There are a number of neutron sources that are available both for thermal and fast NR. Unfortunately, all of them have a number of drawbacks. Research nuclear reactors provide high intensity thermal neutron beams, but because of thermalization, their fast neutron flux is very poor. In addition, nuclear reactors have a high capital cost and have limited facilities (availability and location).

Deuterium–Deuterium (DD) neutron generators emit neutrons with an average energy of approximately 2.5 MeV and offer on/off switching of the emitted neutrons. In addition, these generators have a compact size and a relatively low neutron flux; however, their lifetime is extremely short (usually no more than 2000 h). Deuterium–Tritium (DT) neutron generators produce neutrons with an average energy of approximately 14 MeV and, for this reason, are mainly suitable for fast neutron radiography. DT neutron generators have the same drawbacks and benefits as DD generators, except for the fact that the neutron flux of DT generators is approximately two orders of magnitude higher than that of DD generators. Accelerator-driven neutron beams also offer on/off switching of the emitted neutrons and provide higher intensity neutron beams that are mainly suitable for epithermal or fast neutron imaging. Neither accelerator is inexpensive, but both usually require a series of ancillary systems, which may occupy a large space [10–13].

A variety of commercially available isotopic neutron sources are suitable for both *in situ* fast and thermal radiography. Usually, these neutron sources emit a low intensity of neutrons, require adequate shielding and represent a major waste-disposal problem. However, isotopic neutron sources can be easily incorporated in transportable radiography units and, for this reason, have mostly found application where maximum portability is required. ^{252}Cf and ^{241}Am/Be are the most commonly used isotopic sources for radiography purposes. ^{252}Cf has a neutron emission rate and average neutron energy of approximately 2.3×10^6 s^{-1} per μg and 2.3 MeV, respectively. ^{252}Cf is best for thermal NR because of its low average emitted neutron energy and small size, but unfortunately, it has a short half-life (2.6 years) and emits 1.3×10^7 photons s^{-1} per μg with a mean energy of 0.8 MeV [14].

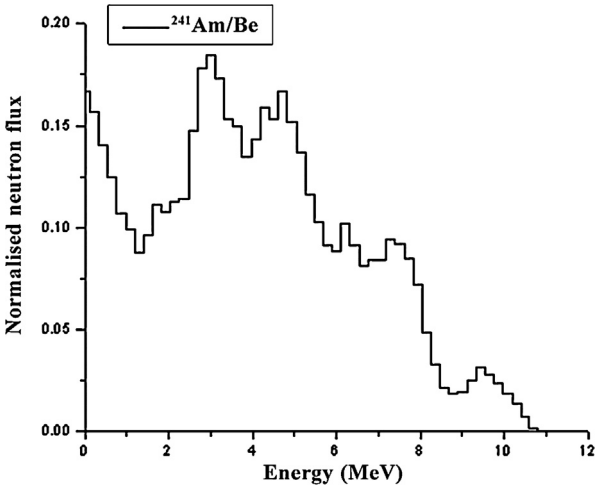

Fig. 1. Normalized neutron spectrum for ^{241}Am/Be.

For the purposes of this study, the ^{241}Am/Be neutron source is used. ^{241}Am/Be with a long half-life (432.7 years) emits approximately 2.7×10^6 s^{-1} per Ci with an average neutron energy of approximately 4.5 MeV (Fig. 1). Additionally, the ^{241}Am/Be neutron source emits low energy photons with energies of 60 keV (almost 36% of decays) and 14 keV (approximately 42% of decays) [15,16].

2.2. Thermal neutron radiography design

In any radiography system, the collimator ratio (L/D), where L is the length of the collimator and D is the diameter of the entrance aperture, defines the quality of the image for a given radiation source type, which is described by the following equations:

$$\phi_i = \frac{\phi_\alpha}{16(L_S/D)^2} \quad (1)$$

and

$$u_g = L_f \frac{D}{L_s} \quad (2)$$

where φ_i is the neutron flux at the image plane, φ_a is the neutron flux at the aperture, L_s is the source to object distance, D is the inlet aperture diameter, u_g is the geometric unsharpness and L_f is the image surface to object distance. In addition, the beam divergence is a

Please cite this article in press as: J.G. Fantidis. Comparison of different geometric configurations and materials for neutron radiography purposes based on a ^{241}Am/Be neutron source, J. Taibah Univ. Sci. (2016), http://dx.doi.org/10.1016/j.jtusci.2016.10.002

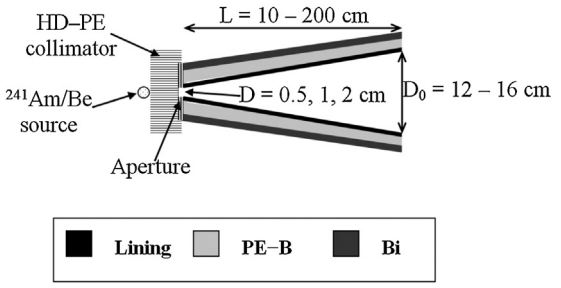

Fig. 2. First geometric configuration for the thermal NR considered facility (not to scale).

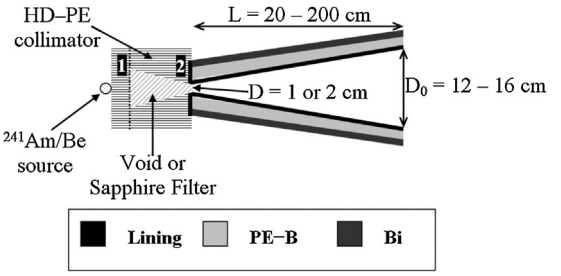

Fig. 3. Second geometric configuration for the thermal NR considered facility (not to scale).

significant measure of the effectiveness of the beam near its periphery and is defined by the equation [11,17]

$$\theta = \tan^{-1}\left(\frac{I}{2L}\right) \tag{3}$$

where θ is the half-angle of the beam divergence, I is the maximum dimension of the image plane (approximately equal to the diameter of its aperture next to the image plane D_0 in the calculation) and L is the length of the collimator.

The imaging quality of a thermal NR system can additionally be characterized by the Thermal Neutron Content (*TNC*), which illustrates the percentage of thermal neutrons within the neutron beam

$$TNC = \frac{\text{thermal neutron flux}}{\text{total neutron flux}} \tag{4}$$

and by the (n/γ) ratio, which describes the relative intensities of the neutron (n) and the photon (γ) components of the beam. According to Hawkesworth, the ratio should be [18]:

$$\frac{n}{\gamma} > 10^4\, n\ \text{cm}^{-2}\,\text{mSv}^{-1} \tag{5}$$

Based on previous articles by Fantidis et al. [8,19,20] and da Silva and Crispim [11], high density polyethylene (HD-PE) is the optimum moderator because it provides the highest thermal neutron flux. In the literature, there are two different concepts for the design of a thermal NR collimator. The first concept only uses a conic divergent collimator [11,19]; the second concept uses two collimators, of which the first is a convergent collimator and the second is a divergent collimator.

Fig. 2 shows the design for the first concept. According to this design, the conic divergent collimator is placed next to the required 4.1 cm of the HD-PE moderator. The most important part of the collimator, the lining, should be made of a neutron absorbing material. In this study, three different materials that are often used as lining materials in thermal NR, namely, Cadmium, Gadolinium and Boral, were considered [8,11,13]. The divergent collimator is composed of a 0.5 cm layer of a lining material covered by a 3.5 cm layer of borated polyethylene (PE-B), while Bismuth (Bi) with 1 cm of thickness is used as the collimator casing. The aperture is composed of three materials: a 0.5 cm-thick layer of lining; a 0.1 cm-thick Indium filter that prevents epithermal neutrons from entering the neutron beam and traveling toward the object; and a 2.4 cm-thick layer of Bi to capture the unwanted gamma-rays.

Fig. 3 illustrates the design of the second concept. This geometrical configuration is similar to that described previously in Ref. [13] with a minor difference in geometry. Fast neutrons from the ^{241}Am/Be source are thermalized using 4.1-cm thick HD-PE (1); thus, the highest thermal neutron flux at the collimator inlet aperture is achieved. The collimator is made of two parts; the first, attached to the HD-PE moderator, is a HD-PE cylinder (2) with a radius of 10 cm and length of 15 cm and incorporates a conic convergent collimator that is made from a single sapphire or has a void with a length of 15 cm and radii of 6 and 1 (or 2) cm. The larger radius is placed near the HD-PE moderator, while the smaller radius is equal to the aperture size (1 or 2 cm). The second part, the conic divergent collimator, is similar to this and was described earlier in the first concept design (Fig. 2).

2.3. Fast neutron radiography design

As in the case of thermal NR, the quality of fast NR imaging is primarily defined by the collimator ratio (*L*/*D*). The geometric unsharpness u_g is specified by equation [21]

$$u_g = \frac{DL_f}{L_\alpha - L_f} \tag{6}$$

where D is the collimator aperture diameter, L_f is the image surface to object distance and L_a is the distance from the aperture to the image plane.

Please cite this article in press as: J.G. Fantidis. Comparison of different geometric configurations and materials for neutron radiography purposes based on a ^{241}Am/Be neutron source, J. Taibah Univ. Sci. (2016), http://dx.doi.org/10.1016/j.jtusci.2016.10.002

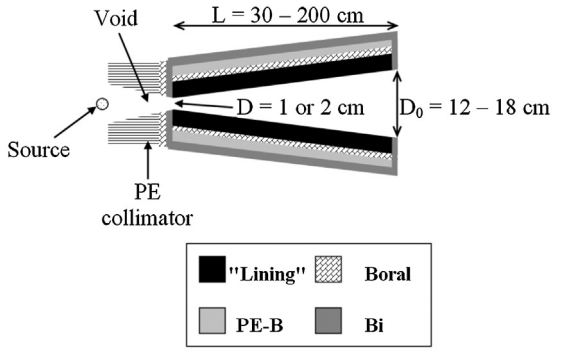

Fig. 4. Aperture geometry and collimator design for fast NR (not to scale).

The imaging quality of a fast NR facility can be further characterized by the Fast Neutron Content (*FNC*), which describes the number of fast neutrons within the neutron beam, as well as by the number of uncollided neutrons that reach at the detector.

$$FNC = \frac{\text{fast neutron flux}}{\text{total neutron flux}} \quad (7)$$

Unfortunately, there are no materials that are strong absorbers of fast neutrons; however, suitable imaging systems can be effectively built and used. According to previous works, iron and tungsten are the best choices for "lining" materials [22]. In this case, the fast neutron collimator is also composed of two parts [8]. The first, a HD-PE cylinder with a radius and length of 10 and 15 cm, respectively, incorporates a void conic convergent collimator and is a combination of four materials (from the inside outwards): 8-cm thick iron (Fe) or Tungsten (W), 0.5-cm thick Boral, 2-cm thick PE-B, and 1.5-cm Bi. In addition, there is a 2-cm thick layer of Bi casing on the front side of the collimator. Between the two collimators, there is an aperture that comprises a combination of two materials: 0.5 cm of Boral and a 1.5 cm-thick layer of Bi (Fig. 4).

3. Results and discussion

3.1. Thermal NR

For the geometric configuration that is illustrated in Fig. 2, system simulations were carried out for variable collimator lengths (L = 10–100 cm); an aperture size equal to 0.5, 1 or 2 cm; variable diameters with the aperture next to the image plane (D_0 = 12–16 cm); and a wide range of divergence angles (θ) of the beam (θ = 4.5–30.9°). The distance between the object and imaging detector (L_f) was considered to be 0.5 cm [18]. The calculated thermal NR parameters, thermal neutron flux (f_{th}) and *TNC* are given in Table 1. The n/γ ratio in all circumstances has values that are at least four orders of magnitude greater than the recommended value. The f_{th} per source particle was calculated with the aid of the MCNP4B code using the F2 tally that gives the averaged neutron flux over a surface in neutrons cm^{-2} per starting neutron. Calculations were performed with NPS of up to 2×10^7 neutrons, yielding an accuracy of <2%. According to the results, the Gadolinium lining offers both the highest f_{th} and maximum *TNC*, while the Cadmium lining gives better results than the Boral lining.

In the case of the two collimator designs, the proposed facility has a variable collimator length (L = 10–100 cm), changeable diameter of its aperture close to the image plane (D_0 = 12–16 cm), and variable divergence angle (θ) of the beam (θ = 2.3–8.5°), while the inlet aperture is 1 or 2 cm. The distance between the object and imaging detector (L_f) was considered to be 0.5 cm [18]. Simulations were carried out with a NPS of up to 6×10^7 neutrons, yielding an accuracy of <2%. The f_{th} and *TNC* parameters were calculated are shown in Table 2 for different lining materials. The n/γ ratio is omitted because it has values that are at least two orders of magnitude greater than the recommended value. Based on the simulation data, the Boral lining has the maximum f_{th} and *TNC* and the Cadmium and Gadolinium linings have similar results. The *TNC* has similar values for the three types of linings. The comparison of the two designs reveals that the presence of the first converging collimator drastically improves both the f_{th} and *TNC*. In the case of the Cadmium, Gadolinium and Boral linings, the f_{th} values increased by factors of 1.36–2.01, 1.28–2.03 and 1.74–2.38, respectively. Similarly, there is a great improvement in the *TNC* values. Without the converging collimator, *TNC* fluctuates between 0.39–1.66%, 0.41–1.65% and 0.36–1.64%, while with the converging collimator, it varies from 4.11–6.57%, 4.07–6.49% and 4.19–7.45% for Cadmium, Gadolinium and Boral linings, respectively.

If there is a requirement for higher *TNC* values, the converging collimator could be filled with a fast neutron filter, such as sapphire [23]. The f_{th} and *TNC* parameters were also calculated for the Boral lining and for three different sapphire filter thicknesses (5, 10 and 15 cm). The results are given in Table 3 and show that the presence of sapphire has the consequence of an average reduction of the f_{th} by a factor of 1.22, 1.45 and 1.72 for thicknesses of 5, 10 and 15 cm, respectively. The *TNC* varies in the range of 8.96–14.63%, 12.47–25.86%, and 12.79–37.65% for 5, 10 and 15 cm sapphire filters, respectively.

Please cite this article in press as: J.G. Fantidis. Comparison of different geometric configurations and materials for neutron radiography purposes based on a ^{241}Am/Be neutron source, J. Taibah Univ. Sci. (2016), http://dx.doi.org/10.1016/j.jtusci.2016.10.002

Table 1
Thermal NR calculated parameters for different *L/D* values for the first geometrical configuration.

L (cm)	*L/D*	D_0 (cm)	θ (°)	U_g (cm)	Gadolinium lining		Cadmium lining		Boral lining	
					f_{th} (n cm^{-2} s^{-1})	*TNC* (%)	f_{th} (n cm^{-2} s^{-1})	*TNC* (%)	f_{th} (n cm^{-2} s^{-1})	*TNC* (%)
10	20	12	30.9	2.50E−2	1.18E−6	0.23	1.14E−6	0.22	9.50E−7	0.19
12.5	25	12	25.6	2.00E−2	8.10E−7	0.22	7.86E−7	0.22	6.89E−7	0.19
15	30	14	25	1.66E−2	4.77E−7	0.19	4.68E−7	0.18	3.61E−7	0.14
20	40	16	21.8	1.25E−2	2.87E−7	0.20	2.83E−7	0.20	2.21E−7	0.16
25	50	16	17.7	1.00E−2	1.60E−7	0.18	1.43E−7	0.16	1.07E−7	0.12
20	20	12	16.7	2.50E−2	7.33E−7	0.45	7.08E−7	0.44	5.85E−7	0.36
25	25	12	13.5	2.00E−2	4.42E−7	0.43	4.41E−7	0.43	3.61E−7	0.35
30	30	14	13.1	1.66E−2	2.84E−7	0.41	2.71E−7	0.39	2.46E−7	0.36
40	40	16	11.3	1.25E−2	1.63E−7	0.44	1.59E−7	0.42	1.43E−7	0.39
50	50	16	9.1	1.00E−2	1.09E−7	0.49	1.08E−7	0.49	9.70E−8	0.45
40	20	12	8.5	2.50E−2	5.64E−7	1.25	5.56E−7	1.23	5.54E−7	1.26
50	25	12	6.8	2.00E−2	3.65E−7	1.34	3.63E−7	1.35	3.46E−7	1.34
60	30	14	6.6	1.66E−2	2.74E−7	1.50	2.67E−7	1.48	2.44E−7	1.40
80	40	16	5.7	1.25E−2	1.52E−7	1.59	1.49E−7	1.56	1.41E−7	1.54
100	50	16	4.5	1.00E−2	9.59E−8	1.65	9.56E−8	1.66	9.16E−8	1.64

Table 2
Thermal NR calculated parameters for different *L/D* values for the second geometrical configuration.

L (cm)	*L/D*	D_0 (cm)	θ (°)	U_g (cm)	Gadolinium lining		Cadmium lining		Boral lining	
					f_{th} (n cm^{-2} s^{-1})	*TNC* (%)	f_{th} (n cm^{-2} s^{-1})	*TNC* (%)	f_{th} (n cm^{-2} s^{-1})	*TNC* (%)
20	20	12	8.5	2.50E−2	9.44E−7	4.83	9.63E−7	4.90	1.02E−6	5.30
25	25	12	6.8	2.00E−2	7.98E−7	5.46	7.62E−7	5.42	8.58E−7	6.01
30	30	14	6.7	1.66E−2	5.30E−7	5.38	5.27E−7	5.49	5.83E−7	6.18
40	40	16	5.7	1.25E−2	3.31E−7	5.73	3.19E−7	5.62	3.35E−7	5.93
50	50	16	4.6	1.00E−2	2.04E−7	4.85	2.05E−7	4.91	2.26E−7	5.41
40	20	12	4.3	2.50E−2	1.01E−6	6.49	1.02E−6	6.57	1.15E−6	7.45
50	25	12	3.4	2.00E−2	7.10E−7	5.68	7.06E−7	5.73	8.25E−7	6.65
60	30	14	3.3	1.66E−2	4.94E−7	5.57	4.96E−7	5.70	5.47E−7	6.26
80	40	16	2.8	1.25E−2	3.00E−7	5.23	2.98E−7	5.25	3.21E−7	5.64
100	50	16	2.3	1.00E−2	1.90E−7	4.07	1.92E−7	4.11	1.94E−7	4.19

Table 3
Thermal NR calculated parameters for different *L/D* values the second geometrical configuration with 5, 10 and 15 cm single sapphire filter.

L (cm)	*L/D*	Without Sapphire filter		With 5 cm Sapphire filter		With 10 cm Sapphire filte		With 15 cm Sapphire filter	
		f_{th} (n cm^{-2} s^{-1})	*TNC* (%)	f_{th} (n cm^{-2} s^{-1})	*TNC* (%)	f_{th} (n cm^{-2} s^{-1})	*TNC* (%)	f_{th} (n cm^{-2} s^{-1})	*TNC* (%)
20	20	1.02E−6	5.30	8.42E−7	8.96	7.10E−7	12.47	5.98E−7	12.76
25	25	8.58E−7	6.01	7.07E−7	11.41	5.97E−7	16.22	5.01E−7	16.63
30	30	5.83E−7	6.18	4.77E−7	10.43	4.05E−7	15.92	3.40E−7	17.11
40	40	3.35E−7	5.93	2.73E−7	10.52	2.33E−7	17.15	1.95E−7	19.51
50	50	2.26E−7	5.41	1.86E−7	10.42	1.56E−7	17.59	1.31E−7	22.12
40	20	1.15E−6	7.45	9.47E−7	14.63	7.99E−7	25.86	6.73E−7	36.36
50	25	8.25E−7	6.65	6.72E−7	13.61	5.73E−7	25.20	4.82E−7	37.65
60	30	5.47E−7	6.26	4.48E−7	13.05	3.80E−7	24.38	3.20E−7	36.67
80	40	3.21E−7	5.64	2.64E−7	12.16	2.23E−7	23.93	1.87E−7	36.66
100	50	1.94E−7	4.19	1.70E−7	10.09	1.35E−7	19.63	1.13E−7	33.63

Please cite this article in press as: J.G. Fantidis. Comparison of different geometric configurations and materials for neutron radiography purposes based on a ^{241}Am/Be neutron source, J. Taibah Univ. Sci. (2016), http://dx.doi.org/10.1016/j.jtusci.2016.10.002

Table 4
Fast NR calculated parameters for different *L*/*D* values.

L (cm)	*L*/*D*	D_0 (cm)	θ (°)	U_g (cm)			Iron collimator			Tungsten collimator		
				L_f = 5 cm	L_f = 15 cm	L_f = 25 cm	F_F (n cm^{-2} s^{-1})	FNC (%)	Uncollided f_F (%)	F_F (n cm^{-2} s^{-1})	FNC (%)	Uncollided f_F (%)
30	30	12	11.31	2.00E−1	1.00E+0	5.00E+0	2.58E−5	93.82	75.02	2.42E−5	95.41	80.03
40	40	12	8.53	1.43E−1	6.00E−1	1.67E+0	1.98E−5	96.41	87.73	1.90E−5	97.26	91.44
50	50	14	7.97	1.11E−1	4.29E−1	1.00E+0	1.85E−5	97.31	93.46	1.81E−5	98.00	95.93
60	60	14	6.65	9.09E−2	3.33E−1	7.14E−1	1.38E−5	97.92	95.79	1.36E−5	98.29	97.15
70	70	16	6.52	7.69E−2	2.73E−1	5.56E−1	1.07E−5	97.98	96.60	1.06E−5	98.39	97.70
80	80	16	5.71	6.67E−2	2.31E−1	4.55E−1	8.56E−6	98.35	97.42	8.49E−6	98.55	98.33
90	90	18	5.71	5.88E−2	2.00E−1	3.85E−1	7.02E−6	98.39	97.65	6.97E−6	98.55	98.44
100	100	18	5.14	5.26E−2	1.76E−1	3.33E−1	5.84E−6	98.47	98.20	5.81E−6	98.61	98.67
60	30	12	5.71	1.82E−1	6.67E−1	1.43E+0	1.38E−5	97.89	95.59	1.37E−5	98.30	96.78
80	40	12	4.29	1.33E−1	4.62E−1	9.09E−1	8.55E−6	98.44	97.57	8.50E−6	98.51	98.20
100	50	14	4.00	1.05E−1	3.53E−1	6.67E−1	5.84E−6	98.48	98.24	5.83E−6	98.60	98.35
120	60	14	3.34	8.70E−2	2.86E−1	5.26E−1	4.27E−6	98.52	97.97	4.26E−6	98.63	98.16
140	70	16	3.27	7.41E−2	2.40E−1	4.35E−1	3.24E−6	98.60	98.19	3.24E−6	98.61	98.20
160	80	16	2.86	6.45E−2	2.07E−1	3.70E−1	2.55E−6	98.57	98.16	2.55E−6	98.64	98.23
180	90	18	2.86	5.71E−2	1.82E−1	3.23E−1	2.06E−6	98.37	98.20	2.06E−6	98.55	98.24
200	100	18	2.58	5.13E−2	1.62E−1	2.86E−1	1.69E−6	98.65	98.34	1.70E−6	98.68	98.37

3.2. Fast NR

Based on the fact that the ^{241}Am/Be source emits neutrons with an average energy of 4.5 MeV, the source was further studied with the MCNP4B code for fast NR. The F2 tally was used to calculate the fast neutron fluxes (f_F) per source particle for a total number of histories per starting neutron of up to 5×10^6 neutrons, yielding an accuracy of <0.2% in the calculations. The facility was studied with a second collimator that had a variable length (L = 30–200 cm), aperture diameter of 1 or 2 cm, aperture diameter next to the image plane (D_0 = 12–18 cm) and divergence angle (θ) of the beam (θ = 2.6–11.3°). The detector was placed at the end of the object. The object was considered to have 5, 15 or 25 cm thicknesses (t).

The f_F, *FNC* and uncollided f_F that characterizes the fast NR are given in Table 4 for iron and tungsten collimators. From Table 4, it is obvious that except for the cases with a small collimator length (L = 30–50 cm), the two materials give similar results. The uncollided f_F that characterizes the beam quality ranges between 75.02 and 98.54% for the Fe collimator and between 80.03 and 98.67% for the W collimator. The *FNC* fluctuates from 93.82 up to 98.65% for the iron collimator, while the corresponding values using the tungsten collimator ranges between 95.41 and 98.68%, yielding a neutron beam that is suitable for fast NR.

4. Conclusions

A ^{241}Am/Be neutron source has been simulated for thermal and fast NR purposes using the MCNP4B Monte Carlo code. For thermal NR, two different geometrical configurations and three different materials have been considered as lining materials. In the case when there is only a divergent collimator, the Gadolinium lining provides the highest f_{th} and maximum *TNC*. According to the obtained results, the introduction of a convergent collimator in front of the divergent collimator improves both the f_{th} and the *TNC* to a great extent. In this case, the Boral lining offers better values both for the f_{th} and *TNC*. The use of a sapphire fast neutron filter in the convergent collimator has led to an improvement of the *TNC* parameter with relatively small decreases in f_{th}. For fast NR, the two investigated materials, iron and tungsten, gave comparable results and the parameters that characterize the fast NR imaging indicate high-quality neutron beams.

Acknowledgments

The author gratefully acknowledges the anonymous reviewers for their valuable contributions.

Please cite this article in press as: J.G. Fantidis. Comparison of different geometric configurations and materials for neutron radiography purposes based on a ^{241}Am/Be neutron source, J. Taibah Univ. Sci. (2016), http://dx.doi.org/10.1016/j.jtusci.2016.10.002

References

[1] D. Goers, M. Holzapfel, W. Scheifele, E. Lehmann, P. Vontobel, P. Novák, In situ neutron radiography of lithium-ion batteries: the gas evolution on graphite electrodes during the charging, J. Power Sources 130 (2004) 221–226.
[2] L.G.I. Bennett, T.R. Chalovich, W.J. Lewis, Comparison of neutron radiography with other non-destructive techniques for the inspection of CF188 flight control surfaces, IEEE Trans. Nucl. Sci. 52 (2005) 334–337.
[3] J.E. Eberhardt, S. Rainey, R.J. Stevens, B.D. Sowerby, J.R. Tickner, Fast neutron radiography scanner for the detection of contraband in air cargo containers, Appl. Radiat. Isot. 63 (2005) 179–188.
[4] B.D. Sowerby, J.R. Tickner, Recent advances in fast neutron radiography for cargo inspection, Nucl. Instrum. Methods A 580 (2007) 799–802.
[5] P. Vaz, Neutron transport simulation, Radiat. Phys. Chem. 78 (2009) 829–842.
[6] L.D. Poulikakos, M. Sedighi Gilani, D. Derome, I. Jerjen, P. Vontobel, Time resolved analysis of water drainage in porous asphalt concrete using neutron radiography, Appl. Radiat. Isot. 77 (2013) 5–13.
[7] W.A. el Bar, I.M. Imbaby, A.K. Hussein, Development and characterization of a neutron tomography system for a research reactor, J. Taibah Univ. Sci. 10 (2016) 195–204.
[8] J.G. Fantidis, G.E. Nicolaou, N.F. Tsagas, Optimization study of a transportable neutron radiography unit based on a compact neutron generator, Nucl. Instrum. Methods A 618 (2010) 331–335.
[9] J.F. Briesmeister, MCNP4B MCNPTM – A General Monte Carlo N-particle Transport Code, Version 4B LA-12625-M Manual, 1997.
[10] G. MacGillivray, Imaging with neutrons: the other penetrating radiation, Proc. SPIE 4142 (2000) 48.
[11] A.X. da Silva, V.R. Crispim, Study of a neutron radiography system using ^{252}Cf neutron source, Radiat. Phys. Chem. 61 (2001) 515–517.
[12] H. Jafari, S.A.H. Feghhi, Design and simulation of neutron radiography system based on ^{241}Am–Be source, Radiat. Phys. Chem. 81 (2012) 506–511.
[13] J.G. Fantidis, D.V. Bandekas, N. Vordos, The replacement of research reactors with a compact proton Linac for neutron radiography, Radiat. Phys. Chem. 86 (2013) 74–78.
[14] V.V. Verbinski, H. Weber, R.E. Sund, Prompt gamma rays from ^{235}U(n, f), ^{239}Pu and spontaneous fission of ^{252}Cf, Phys. Rev. C 7 (3) (1973) 1173.
[15] U. Pujala, et al., Radiat. Prot. Environ. 34 (4) (2011) 262.
[16] A.A. Naqvi, M.M. Nagadi, Performance comparison of an ^{241}Am-Be neutron source-based PGNAA setup with the KFUPM PGNAA setup, J. Radioanal. Nucl. Chem. 260 (3) (2004) 641–646.
[17] G.M. MacGillivray, Neutron Radiography Collimator Design. Nray Services Inc, RR#1 Petawawa, Ontario, Canada. Available at: http://stephenwclarke.com/nsi/nray/images/collimatordesign.pdf.
[18] M.R. Hawkesworth, Neutron radiography: equipment and methods, At. Energy Rev. 15 (1977) 169–220.
[19] J.G. Fantidis, G.E. Nicolaou, N.F. Tsagas, A transportable neutron radiography system, J. Radioanal. Nucl. Chem. 284 (2010) 479–484.
[20] J.G. Fantidis, D.V. Bandekas, C. Potolias, N. Vordos, Fast and thermal neutron radiographies based on a compact neutron generator, J. Theor. Appl. Phys. 6 (2012) 20.
[21] H. Berger, F. Iddings, Neutron Radiography, A State-of-the-Art Report, Nondestuctive Testing Information Analysis Center, 1998.
[22] E.M.A. Hussein, Handbook on Radiation Probing, Gauging, Imaging and Analysis Volume II Applications and Design, Kluwer Academic Publishers, 2004.
[23] D.F.R. Mildner, G.P. Lamaze, Neutron transmission of single-crystal sapphire, J. Appl. Crystallogr. 31 (1998) 835–840.

Please cite this article in press as: J.G. Fantidis. Comparison of different geometric configurations and materials for neutron radiography purposes based on a ^{241}Am/Be neutron source, J. Taibah Univ. Sci. (2016), http://dx.doi.org/10.1016/j.jtusci.2016.10.002